Bulletin of the Seismological Society of America, Vol. 95, No. 6, pp. 2297–2317, December 2005, doi: 10.1785/0120040065

Assessment of Site Effects on Seismic Motion in Ashigara Valley, Japan

by Tomiichi Uetake and Kazuyoshi Kudo

Abstract We compared site amplifications at rock sites and sediment sites of Ashigara Valley, Japan, using ground-motion data from five remote (>700 km) large (>M 7) events. The use of remote large events is advantageous to estimating site factors because the source and path effects are considered to be common with a sufficient accuracy and the ground motions will cover a wide-frequency band. Ground motions at both sediment and rock sites were coherent in frequencies lower than 0.1 Hz. This means that the wavelength in these frequencies is longer than the size of the valley (12 km long and 5 km wide). Site amplification factors were determined by taking spectral ratios with reference to one rock outcrop site. The amplification factors of sediment sites deviated 2–10 times with respect to the rock site in the frequency range higher than 0.1 Hz, in which significant peaks at about 1–2 Hz were found at most sites. These dominant amplifications in sedimentary basin are most essential for assessing earthquake hazard in the region. For sediment sites, the peak frequencies of spectral ratios to the rock sites were stable for different events and coincided with those of horizontal to vertical spectral ratios for the *S*-wave portion and those of relative site factors estimated separately by the generalized inversion method using local small-events data in the frequency range higher than 2 Hz. Although spectral ratios for frequencies lower than about 1 Hz should be affected by 3D basin structure, 1D *S*-wave responses represent the amplification of ground motion in the sediment sites for frequencies higher than 2 Hz.

Introduction

The importance of site effects on seismic motion has been realized since the early stages of seismology (e.g., Imamura, 1929; Ishimoto, 1932). Since then, various studies have been conducted. However, it is only recently that quantitative studies have been conducted using strong-motion array data. Several methods have been proposed for evaluating site effects by using ground-motion records, such as soil-to-rock spectral ratios (e.g., Borchert, 1970), a generalized inversion (e.g., Andrews, 1982; Iwata and Irikura, 1988; Boatwright *et al.*, 1991), and horizontal-to-vertical spectral ratios (e.g., Nakamura, 1988; Lermo and Chavez-Garcia, 1993; Field and Jacob, 1995; Yamazaki and Ansary, 1997). Because of the assumptions in these methods and a limitation in data, these methods are also limited in accuracy or applicability. Therefore, a comparative study of these methods on one area will be useful to validate the applicability of each method to other sites (e.g., Field and Jacob, 1995; Riepl *et al.*, 1998). The first method practically gives reliable but relative amplification factors at a site, as a function of frequency. This method, however, requires that the distance from a reference site to a target site be close enough compared with the source distance, because it assumes the same source and path effects. The generalized inversion method has an advantage in that it simultaneously gives source, path, and site factors. This method is excellent in understanding absolute amplification/deamplification of body waves (*S*-wave) at a site; however, uncertainties still remain because of assumptions on source radiation pattern, geometrical spreading factor, and so on. A common issue for the spectral ratio method and the generalized inversion method is the selection of a reference site. The third method using a horizontal-to-vertical spectral ratio is convenient in cases where no reference site is available. However, there is still some controversy on its reliability.

We used data from remote large events to discriminate empirical site responses in the sedimentary basin by the spectral ratio method, because both source and path effects are assumed to be common with sufficient accuracy and the ground motions contain a wide frequency band. From a similar viewpoint, Sasatani *et al.* (1992) used the events immediately beneath the site at intermediate depth to evaluate the basin effects.

Obtaining horizontal-to-vertical spectral ratios using the same data sets, we examined the reliability of this method for empirical site effects. Site amplification factors are also estimated by the generalized inversion method (e.g., Iwata and Irikura, 1988) using local events near Ashigara valley. Through a comparative study of these results, we will con-

firm that the spectral ratio method using remote large-event data is advantageous.

Data

Ashigara Valley is a sediment-filled valley with middle-sized dimensions (12 km long and 5 km wide) located in the western Kanagawa Prefecture, Japan. By historical documents since 1600, we note that this region has been severely damaged by several large earthquakes. The most recent devastating event was the 1923 Kanto earthquake. The valley is surrounded by the Hakone Volcano in the west, Tanzawa Mountains in the north, ans Oiso Hills in the east, and it opens to Sagami Bay in the south. The Kozu-Matsuda and Kannawa active fault systems (e.g., Yamazaki, 1992) are indicated at the east and north margins of the basin. For the most part, we used data acquired at the Ashigara valley strong-motion accelerograph array (Kudo and Shima, 1988; Kudo *et al.*, 1988) installed and maintained by Earthquake Research Institute (ERI), University of Tokyo. The ERI deployed a strong-motion accelerograph array in the sedimentary basins and in rock outcrops at surrounding mountains to study the effects of surface geology (ESG) on seismic motions. The strong-motion observation network used in this study is shown in Figure 1. The network consists of 6 rock outcrop sites surrounding the valley and 15 sediment sites, including temporal stations, in the sedimentary basin. The Kuno area, which is located in the west margin of the valley, was selected as the international test site of the ESG study. Strong-motion records from the 1990 Odawara earthquake (M_{JMA} 5.3) were used in the blind prediction studies (Kudo, 1992; Kudo and Sawada, 1998). The rock site KNO and the sediment sites KNP and KNS were used in the blind prediction study with the different station codes, namely, KR1, KS1, and KS2, respectively. The geology of the rock sites is complex; HYK, KNO, and SJJ are andesite of Quaternary and HSR, AKD, and KHZ are tuff breccia, basalt, and mudstone of Tertiary, respectively. The sediment sites are also on various different geological conditions. KNP, KDW, and NGW are on the Kanto loam (volcanic sandy sediments), KRD and KNS are on humus soils, and other sediment stations are on sandy soils of Quaternary deposits.

We analyzed data sets obtained during the 1993 Kushiro-Oki earthquake (M_{JMA} 7.5), the 1994 Near Vladivostok earthquake (M_{JMA} 7.6), the 1994 Hokkaido Toho-Oki (Shikotan) earthquake (M_{JMA} 8.2), the 1994 Sanriku Haruka-Oki earthquake (M_{JMA} 7.6), and the 2000 Trishima-Kinkai earthquake (M_{JMA} 7.2). Locations of the epicenters are also shown in Figure 1. Earthquake parameters determined by the Japan Meteorological Agency (JMA) are shown in Table 1. The epicenters of these earthquakes are very distant from Ashigara Valley, so that we can expect to have plane incident wave and the common source and path effects within the network. The observed peak ground accelerations (PGAs) are listed in Table 2. Because the PGAs were mostly small, we can assume linear site responses. We should note that a few sites (JNI, KDW, and NGW) could retrieve the ground motions during one or two events. The PGA ratios for sediment to rock sites are between 3 and 5. Amplification factors of sediment sites KNS, NRD, and TKD are quite large compared with the others, and the amplification factor of HYK is the largest among the rock sites.

For the generalized inversion analysis using small events, we used 19 ERI stations, 4 K-NET (Kinoshita, 1998) stations deployed by the National Research Institute for Earth Science and Disaster Prevention (NIED), 6 stations deployed by the Central Research Institute of Electric Power Industry (CRIEPI), and 2 stations maintained by The Tokyo Electric Power Co. Ltd. (TEPCO). Shallow events with magnitudes from 4.0 to 5.5 were selected as shown in Table 3, and the list of station-event matrices is shown in Table 4. We classified the sites simply as rock and sediment, indicated by roman and italic letters, respectively, in Tables 2 and 4, based on their surface geology and irrespective of their *S*-wave velocities or thickness of surface layers. The locations of observation stations and epicenters are shown in Figure 2. Epicentral distances are from 12 to 44 km, and are within 2.5 times the source depths.

The instruments of the ERI stations use force-balanced accelerometers. They have flat responses from direct 0 to 30 Hz (100-Hz sampling), with clipping levels at 2000 cm/sec/sec. Most digitizers of these instruments are 16 bits, although 14 bits are used for the real part whereas the rest, 2 bits, was used for gain-ranging ($\times 1$, $\times 4$, $\times 16$); that is, the least significant acceleration is 0.015 cm/sec/sec for acceleration less than 125 cm/sec/sec. Clocks of the recording systems were adjusted every 12 hr in a day by time signals received from broadcasting services of FM radio. In 1998, most accelerographs in Ashigara Valley were replaced to the K-NET95 type seismometers (24-bit digitizer; Kinoshita, 1998). The K-NET95 type seismometer has the same instrumental response as the older one and uses the time code produced by Global Positioning System (GPS) timer. Therefore, the quality of data from event L5 is much higher than the others. Different types of accelerometers have been used at the stations of CRIEPI and TEPCO, but the instrumental responses are almost equal in the frequency range from 0.1 to 20 Hz.

Waveform Features of Large Events

We analyzed the data from the five large events in Table 1. In general, acceleration seismograms are suitable to study the characteristics of high-frequency components; however, we used velocity seismograms to study broadband waveform characteristics. To confirm the reliability of low-frequency contents in the following analysis, we compared our records with that of STS-1 at near distance. Figure 3 shows the site locations, the comparison of velocity waveforms of strong motions integrated without filter (YGS) and the STS-1 (JIZ) record, and the spectra comparisons. Even in the worst case (east–west), we may use higher-frequency

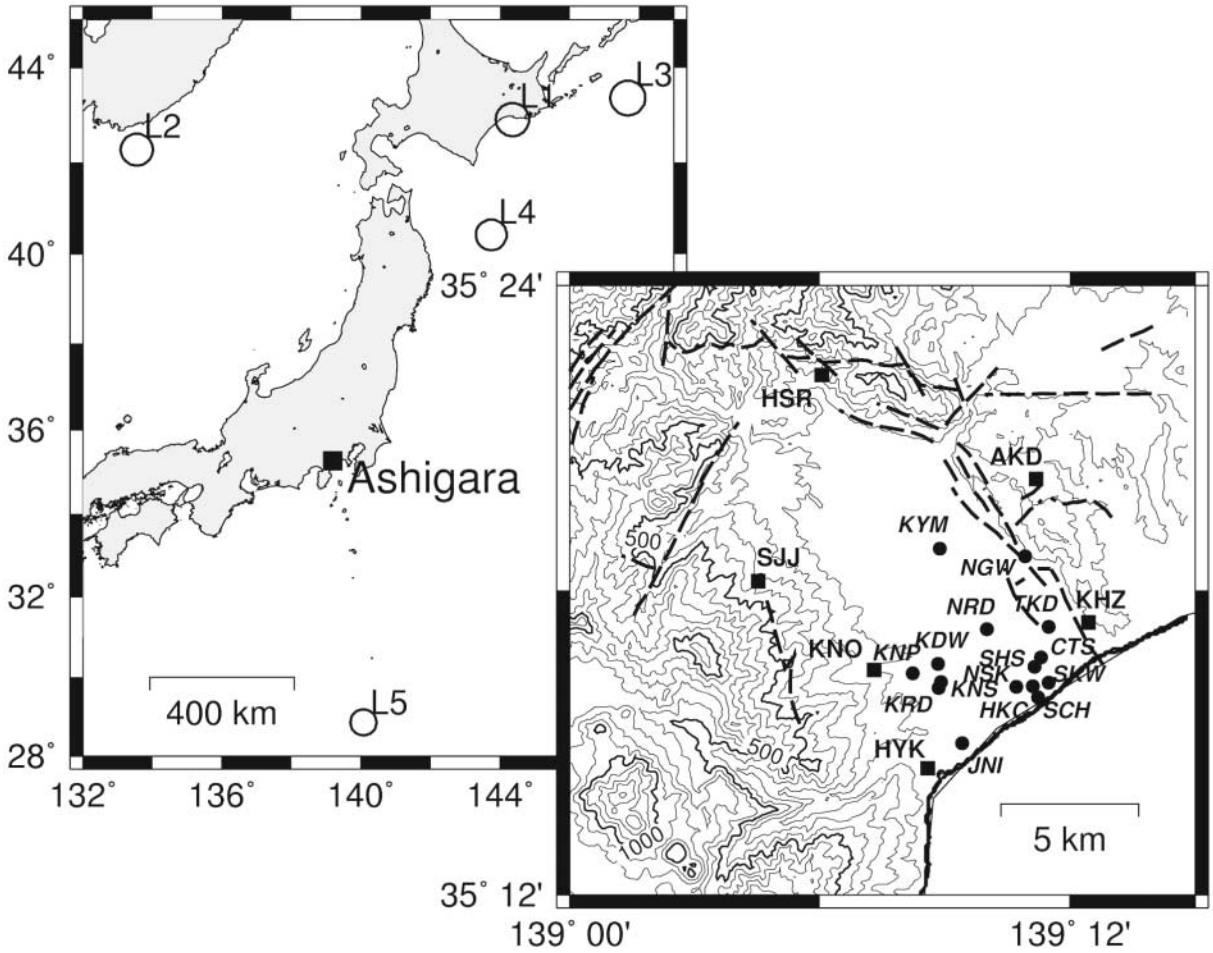

Figure 1. Epicenters of remote large events used in this study and the observation network in Ashigara Valley deployed by the Earthquake Research Institute, University of Tokyo. Station names in roman and italic letters indicate rock and sediment sites, respectively. Broken lines indicate active fault lines. The circles with numbers indicate the epicenters, and the numbers express the locations of earthquakes listed in Table 1.

Table 1
List of Remote Large Earthquakes Used in This Study

Earthquake No.	Origin Time (JST) yyyy/mm/dd	hr:min:sec	Latitude (° N)	Longitude (° E)	Depth (km)	M_{JMA}	M_w	Epicentral Distance (km)	Back Azimuth (°)
L1	1993/01/15	20:06:07.2	42.917	144.357	101	7.5	7.6	962	30
L2	1994/07/22	03:36:31.5	42.277	133.550	552	7.6	7.3	916	326
L3	1994/10/04	22:22:56.9	43.372	147.678	28	8.2	8.3	1162	42
L4	1994/12/28	21:19:20.9	40.427	143.748	0	7.6	7.8	702	37
L5	2000/08/06	16:27:13.3	28.817	140.089	444	7.2	7.4	721	173

Source parameters were determined by the Japan Meteorological Agency. Epicentral distances and back azimuths were calculated from the KNO station. M_w values were determined by the U.S. Geological Survey.

motion than 0.04 Hz. Numerical integration by Fast Fourier transform (FFT) was applied to the acceleration records considering the signal-to-noise ratio (S/N) in the low-frequency range. A cosine-tapered, low-cut filter was applied before integration with cutoff frequency of 0.05 Hz for events L1 and L2, 0.02 Hz for event L3, 0.03 Hz for event L4, and 0.04 Hz for event L5. Velocity waveforms are shown in Figure 4. Every velocity waveform shown in Figure 4a–e has a duration longer than 90 sec, and most events were retrieved before the initial *S* arrivals. As is clearly evident in the figures, the amplitudes at rock sites (indicated by roman letters) are very small compared with those at sediment sites

Table 2
Peak Ground Accelerations of Observed Records

Station	Peak Ground Acceleration (cm/sec/sec)				
	L1	L2	L3	L4	L5
	1993/01/15	1994/07/22	1994/10/04	1994/12/28	2000/08/06
HSR	3.2	2.4	4.5	1.7	1.0
SJJ	—	1.8	4.8	2.2	1.6
AKD	1.8	—	—	1.8	1.0
KNO	2.6	1.8	3.7	2.3	1.3
KHZ	2.5	—	3.5	2.6	1.3
HYK	4.7	1.8	6.7	3.7	1.7
KNP	—	—	15.7	—	—
KNS	10.2	9.0	14.7	—	4.7
KRD	—	—	12.5	7.6	—
KYM	7.7	3.7	7.8	4.2	2.6
NRD	8.8	6.8	14.2	8.4	4.2
TKD	9.4	6.8	20.5	—	8.7
CTS	7.7	5.8	12.0	7.3	4.6
SHS	—	4.5	11.1	7.4	4.8
NSK	5.4	3.8	8.2	5.4	3.2
HKC	—	3.0	9.2	4.7	2.3
SKW	7.3	3.6	10.3	5.6	2.6
SCH	—	—	11.5	5.0	—
JNI	9.4	—	11.7	—	—
KDW	—	—	—	—	5.5
NGW	—	—	—	—	4.5

Earthquake numbers are the same as those in Table 1. The bigger value between the north–south and east–west components is taken as the value in the table. Station codes in roman and italic letters denote rock and sediment sites, respectively.

Table 3
List of Events Used for Generalized Inversions

Earthquake No.	Origin Time (JST)		Latitude (°N)	Longitude (°E)	Depth (km)	M_{IMA}
	yyyy/mm/dd	hr:min:sec				
1	1990/08/05	16:13:02.1	35.207	139.095	13.6	5.3
2	1994/10/04	02:56:00.4	35.480	139.078	23.6	4.4
3	1996/03/06	23:12:27.6	35.471	138.945	19.3	4.6
4	1996/03/06	23:35:28.7	35.473	138.951	19.5	5.5
5	1996/10/25	12:25:17.6	35.452	139.005	22.6	4.7
6	1997/11/04	10:31:08.3	35.249	139.107	14.6	4.1
7	1999/05/22	09:48:15.5	35.456	139.180	20.9	4.3
8	2000/02/11	20:57:04.0	35.496	139.047	16.8	4.4
9	2000/05/02	23:32:59.4	35.300	139.068	15.6	4.0

Source parameters were determined by the Japan Meteorological Agency.

(indicated by italic letters). One exception is event L3, showing similar peak ground velocities (PGVs) almost all sites irrespective of the site geology. The waveforms of event L3 show a clear dispersion of surface waves (Uetake and Kudo, 1998), predominantly in the frequency of 0.03–0.04 Hz. The PGV is mostly controlled by the low-frequency surface waves, but if we pay attention to ground motions for frequencies higher than 0.1 Hz (see Fig. 5a), the same amplification in the sediment site as seen in the other events is found. Bandpass-filtering technique is applied to study the difference of site response for broad-frequency bands. The filtered waveforms of events L3 and L5 are shown in Figure 5. Frequency bands were selected for logarithmically equal width of frequency. Bandpass-filtered waveforms for both events in the frequency range from 0.0464 to 0.1 Hz are very coherent, although they possessed different features for different events, i.e., later arrivals dominate for event L3, whereas pulselike *S* waves are clear for event L5. This suggests that seismic wavelengths in these frequencies are sufficiently longer than the size of the valley and that the S/N of the records are preserved in these low frequencies. In the frequency range from 0.1 to 0.215 Hz, sediment site records are different from those of rock sites with respect to amplitude and phases. Waveforms at sediment sites tend to have larger and longer wavepackets than those at rock sites. However, even though it is a rock site, the KHZ waveform is similar to those of sediment sites. On the other hand, the waveform at sediment site KYM is similar to those of rock sites. In the higher-frequency range of over 0.215 Hz, differences between waveforms from sediment and rock sites become large. The peak values at the low-frequency band appear at the same phase for all stations, but those at the high-frequency band are found at different phases.

Reference Site of Ashigara Valley

Rock types or physical parameters at the observation sites are not the same among the rock outcrop sites of the

Table 4
Data List for Inversion Analysis

Institutions	Station	Latitude (° N)	Longitude (° E)	Earthquake No. 1	2	3	4	5	6	7	8	9	
K-NET	*KNG010*	35.3322	139.3536	—	—	—	—	○	○	○	○	—	4
	KNG012	35.3761	139.2080	—	—	—	—	○	○	○	○	—	4
	KNG013	35.2608	139.1552	—	—	—	—	○	○	○	○	—	4
	KNG014	35.3575	139.0858	—	—	—	—	○	○	○	○	—	4
CRIEPI	MNZ	35.1392	139.1553	—	—	—	—	○	○	○	—	○	4
	JZD	35.3092	139.0286	○	—	○	○	○	○	○	○	○	8
	KND	35.2700	139.1508	○	○	○	○	○	○	○	○	○	9
	KKM	35.2086	139.1439	○	○	○	○	○	○	○	○	○	9
	KZR	35.2464	139.1275	—	—	○	○	○	○	○	○	○	7
	OYM	35.3592	139.0025	○	○	○	○	○	○	○	○	○	9
ERI	AKD	35.3331	139.1894	—	—	○	○	○	—	○	○	○	6
	CTS	35.2744	139.1914	○	○	—	—	○	○	○	—	—	5
	HKC	35.2653	139.1883	—	○	○	○	○	○	—	—	—	5
	HSR	35.3669	139.1039	○	○	○	○	○	○	○	○	○	9
	HYK	35.2383	139.1464	○	○	○	○	○	○	○	○	○	9
	JNI	35.2464	139.1600	—	○	○	○	○	○	—	—	—	5
	KHZ	35.2861	139.2106	○	○	○	○	○	○	—	○	○	8
	KNO	35.2706	139.1250	○	○	○	○	○	○	○	○	○	9
	KNP	35.2696	139.1402	○	○	○	○	○	○	—	—	—	6
	KNS	35.2666	139.1516	○	○	○	○	○	○	○	○	○	9
	KRD	35.2616	139.1506	—	○	○	○	○	○	—	—	—	5
	KYM	35.3103	139.1511	○	○	○	○	○	○	○	○	○	9
	NRD	35.2839	139.1700	○	○	○	○	○	○	○	○	○	9
	NSK	35.2650	139.1817	○	○	○	—	○	○	○	○	○	8
	SCH	35.2616	139.1904	—	○	○	○	○	○	—	—	—	5
	SHS	35.2715	139.1891	—	○	○	○	○	○	—	—	—	5
	SJJ	35.2994	139.0786	○	○	○	○	○	○	○	○	○	9
	SKW	35.2664	139.1947	○	○	○	○	○	○	○	○	○	9
	TKD	35.2847	139.1947	—	○	○	○	○	○	○	○	○	8
TEPCO	*NSG*	35.2878	139.1214	○	—	—	○	○	○	—	—	—	4
	SFJ	35.3692	138.9603	○	—	○	○	—	—	—	—	—	3
	Total			18	21	24	24	30	29	22	21	18	207

Station codes in roman and italic letters denote rock and sediment sites, respectively. The left column lists the observation institutions: K-NET; CRIEPI, The Central Research Institute of Electric Power Industry; ERI, Earthquake Research Institute, University of Tokyo; and TEPCO, Tokyo Electric Power Company.

Ashigara Valley network. By using datasets from events L4 and L5 (see Table 1), which were recorded at all rock sites, we obtained spectral ratios of individual rock sites with respect to the average of all rock sites, as shown in Figure 6. Data over 5 Hz from event L4 were not used because of its low S/N. The deviations of spectral ratios are within a factor of 2 in a wide-frequency band; in particular, it is within 20% in frequencies lower than 0.1 Hz. This implies that the wavelength in this frequency range is longer than the size of irregularities in Ashigara Valley and that the quality of observed records are good, even at very low frequencies. The spectral ratios of horizontal components at KNO and SJJ are close to the average in the broad-frequency range. Those at HSR and AKD are slightly smaller in the intermediate-frequency range (0.1–1.0 Hz); on the other hand, those at HYK and KHZ are larger in the same frequency range. In the high-frequency range over 2 Hz, HSR and HYK show large amplification factors of 2 or 3. These spectral responses at rock sites may be attributed to the effects of weathering rock (Steidl *et al.*, 1996), rock types and/or surface topography.

For the reference site, it is desirable that the spectral response of the site is smooth with respect to frequency and minimum on average compared with others. For these reasons, AKD and SJJ are good choices for the following analysis. Unfortunately, some events could not be retrieved (see Table 2), and so, KNO was finally chosen as the next-best reference site, considering that KNO was also used as a reference site in the ESG blind prediction study (Kudo, 1992; Kudo and Sawada, 1998).

Relative Site Factors Evaluated Using Large-Events Data

In general, Fourier spectra of observed record at station j is represented by,

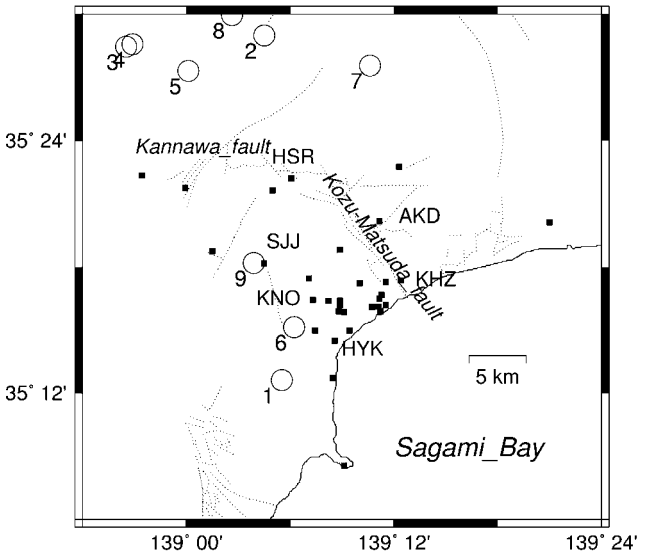

Figure 2. Epicenters and observation stations used for inversion analyses. Open circles show the epicenters. Event numbers are the same as those in Table 3. Filled squares show the observation stations.

$$O_j(f) = S(f) \cdot P_j(f) \cdot G_j(f) \cdot I_j(f), \qquad (1)$$

where, f is frequency, $S(f)$ shows source spectra. $O_j(f)$, $P_j(f)$, $G_j(f)$, and $I_j(f)$ represent observed record, pass effect, site response, and instrumental response of station j, respectively. Assuming that the source and path effects from remote events are common for all stations, and that $I_j(f)$ is also the same for all stations, the spectral ratio of the observed record at a site j to the reference site record 0 gives the relative site response,

$$O_j(f) \,/\, O_0(f) = G_j(f) \,/\, G_0(f). \qquad (2)$$

Expression (2) gives an empirical (relative) amplification factor if an input motion from the base rock is approximately equal for all the stations. Note that, as discussed in the preceding section, KNO was chosen as the next-best reference site.

Spectral ratios of individual events and their overall average are plotted in Figure 7a–c. These spectra were computed using a time window of 81.92 sec, taking the initial part of the *S*-wave arrival. The spectral ratios for stations that recorded more than three events are shown. Data over 5 Hz from event L4 are not plotted because of low S/N and were not included in obtaining the average.

The spectral ratios of every component are stable in a broad-frequency band, irrespective of the event. The spectral ratios of horizontal motions, even for the rock sites, have strong variations against frequency. Significant troughs at about 0.5 Hz appear at almost all north–south (NS) components of rock sites, although it is not clear in the east–west (EW) component. This is due to the spectral peak at about 0.5 Hz of the reference site KNO. In addition, up–down (UD) components show different features, with the rock sites at AKD and KHZ having strong peaks at about 0.2 Hz. Thus, every rock site, including KNO, has local site response. However, their averages are 0.9–1.3 in the frequency range lower than 0.1 Hz and 0.5–2.0 for the rest, except for frequencies higher than 4 Hz at a few sites (HSR, HYK, and SJJ).

At sediment sites, amplification factors in frequencies lower than 0.1 Hz are similar to those at rock sites; however, they increase from about 0.1 Hz, reaching up to 5–10 times at about 1–2 Hz and at higher frequencies. Troughs at about 0.5 Hz in the spectral ratios of almost all sites, both sediment and rock sites, are again probably brought about by the amplification at the reference (KNO) site. Large peaks at about 1 Hz are commonly found for horizontal spectral ratios of sediment sites, and relatively large ratios at low frequencies of 0.15 and 0.35 Hz are roughly three times at the southeast valley (CTS, SHS, NSK, HKC, and SKW). The trough at about 2 Hz and peak at about 3 Hz are also common features of the southeast valley. These peaks cannot be attributed to the spectral response of KNO, because strong peaks or troughs are not found at rock sites. In the up–down component, the spectral ratios are smaller than those of horizontal components but the peak at about 0.2 Hz is very distinct, especially in the southeast valley (CTS, SHS, NSK, HKC, and SKW), including rock sites AKD and KHZ. A predominance of 1-Hz ground motion in Ashigara Valley was suggested by Kawase and Sato (1992), caused by the amplification due to both stratification of quaternary deposits, whose predominant frequency is about 1 Hz, and basin-induced Love waves from the 1987 Chiba-ken Toho-oki earthquake. Spectral ratios of north–south and east–west components are not the same at some sites, especially at KNS. The north–south component KNS/KNO ratio has two significant peaks at about 1 and 2 Hz, whereas the peak at about 1 Hz can not be found in the east–west component. Sato *et al.* (1998) interpreted the difference as a 2D effect of the small-basin structure, and Kudo and Sawada (1998) interpreted it as an effect of anisotropy of volcanic sediments at shallow intermediate layers. Both effects may contribute to this difference.

Spatial distributions of the spectral ratios with respect to KNO are plotted in Figure 8. These figures were made by spatial interpolation of spectral ratios using the surface-gridding algorithms by Smith and Wessel (1990). Horizontal amplification factors are almost homogeneous at 0.1 Hz, gradually becoming large toward the southeast of the valley at 0.2 and 0.5 Hz. At 1 Hz, the amplification factors tend to concentrate at the southeast of valley (NRD, TKD, and CTS). Those of 2 Hz show a rather complex pattern of two dominating areas near TKD and KNS. This amplification pattern roughly corresponds to the surface geology, which is predominantly backmarsh at both sites. Spatial distributions for the UD component show large amplification factors at the rock sites AKD and KHZ and at the sediment sites of southeast valley at 0.2 Hz. This pattern is different from the

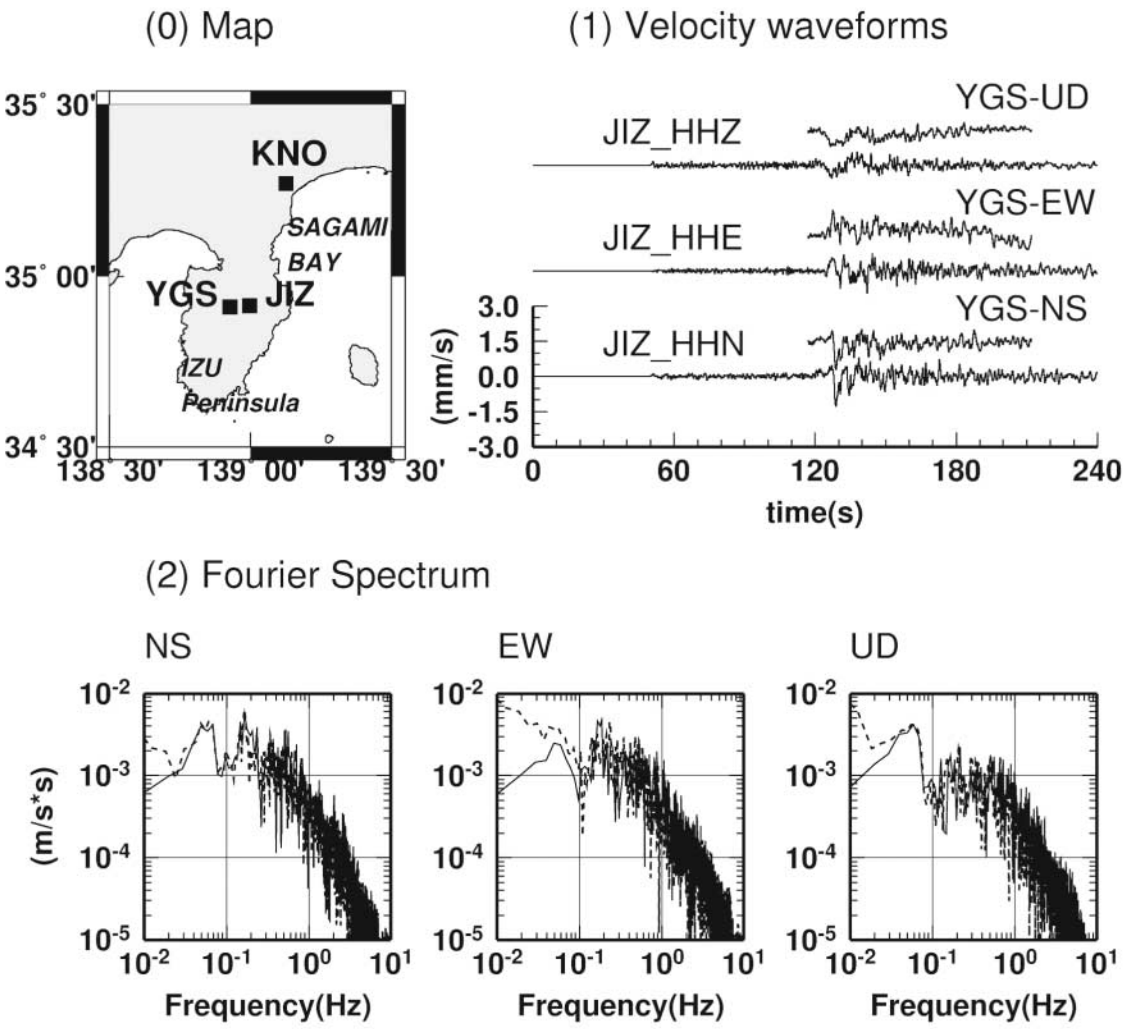

Figure 3. Comparison of velocity waveforms and Fourier spectra observed at YGS and JIZ. These data were obtained from event L5 (2000 Torishima-Kinkai event) in Table 1. Waveforms of YGS were integrated from the original acceleration data. Fourier spectra shown by solid and broken lines are data for JIZ and YGS, respectively. The upper-left map shows the locations of YGS and JIZ stations.

distribution of young sediments. Details for the low frequency up–down motion is outside the scope of this article.

Horizontal to Vertical Spectral Ratio

The method using horizontal-to-vertical spectral ratios (HVRs) of earthquake motions has been proposed as a substitute for site response (e.g., Nakamura, 1988; Lermo and Chavez-Garcia, 1993; Seekins *et al.*, 1996), which employs a simple interpretation that surface vertical motions are *P*-waves converted from *S*-waves at a certain depth and propagated vertically as *P*-waves; therefore, less amplification is expected in a sediment site, whereas surface horizontal motions are amplified because of large changes of *S*-wave velocity in sediments. If the method is valid everywhere, the advantage will be immense for assessing the site effects by using a single station or in an area where a rock reference site cannot be found. However, caution in the use of the method has been indicated by Field and Jacob (1995), Bonilla *et al.* (1997), and Satoh *et al.* (2001), because HVRs tend to underestimate or lose correlation with horizontal spectral ratios (HHRs).

Most of the studies analyzed records by dividing them into their *S*-wave and coda parts to discriminate the wave types that are concerned with the interpretation of the correspondence of HVRs to site responses. However, we obtained HVRs for large events using the same time window to compare with HHRs, which are representative of empirical amplification factors, as shown in Figure 9. The geometrical average of the north–south and east–west components is used as a horizontal value. Spectral ratios are stable in the frequencies higher than roughly 1.0 Hz irrespective of events and site classifications. However, their deviations are very large at frequencies lower than 0.5 Hz, similar to Lermo and

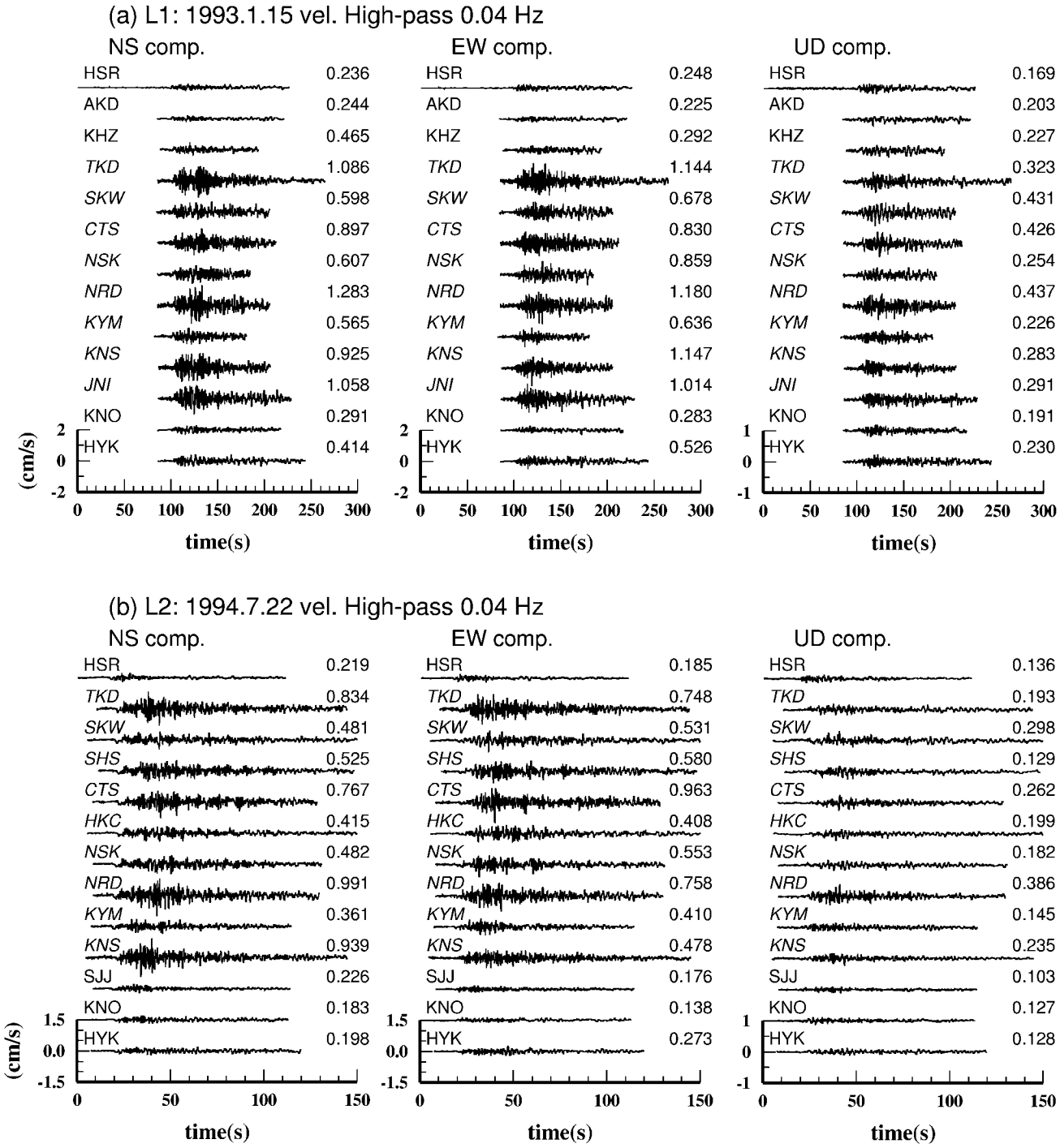

Figure 4. Velocity seismograms of large remote events observed in the Ashigara Valley network. (a) 1993 Kushiro-Oki earthquake (M_{JMA} 7.5). (b) 1994 Near Vladivostok earthquake (M_{JMA} 7.6). (c) 1994 Hokkaido Toho-Oki earthquake (Shikotan) (M_{JMA} 8.2). (d) 1994 Sanriku Haruka-Oki earthquake (M_{JMA} 7.6). (e) 2000 Trishima-Kinkai earthquake (M_{JMA} 7.2). Each trace was integrated from the original acceleration data in the frequency domain. The letters written on the left side of waveforms indicate station code, and the numbers written on the right side of the of waveforms are the PGV values of the waveforms. Station codes in roman and italic letters represent rock and sediment sites, respectively. (*continued*)

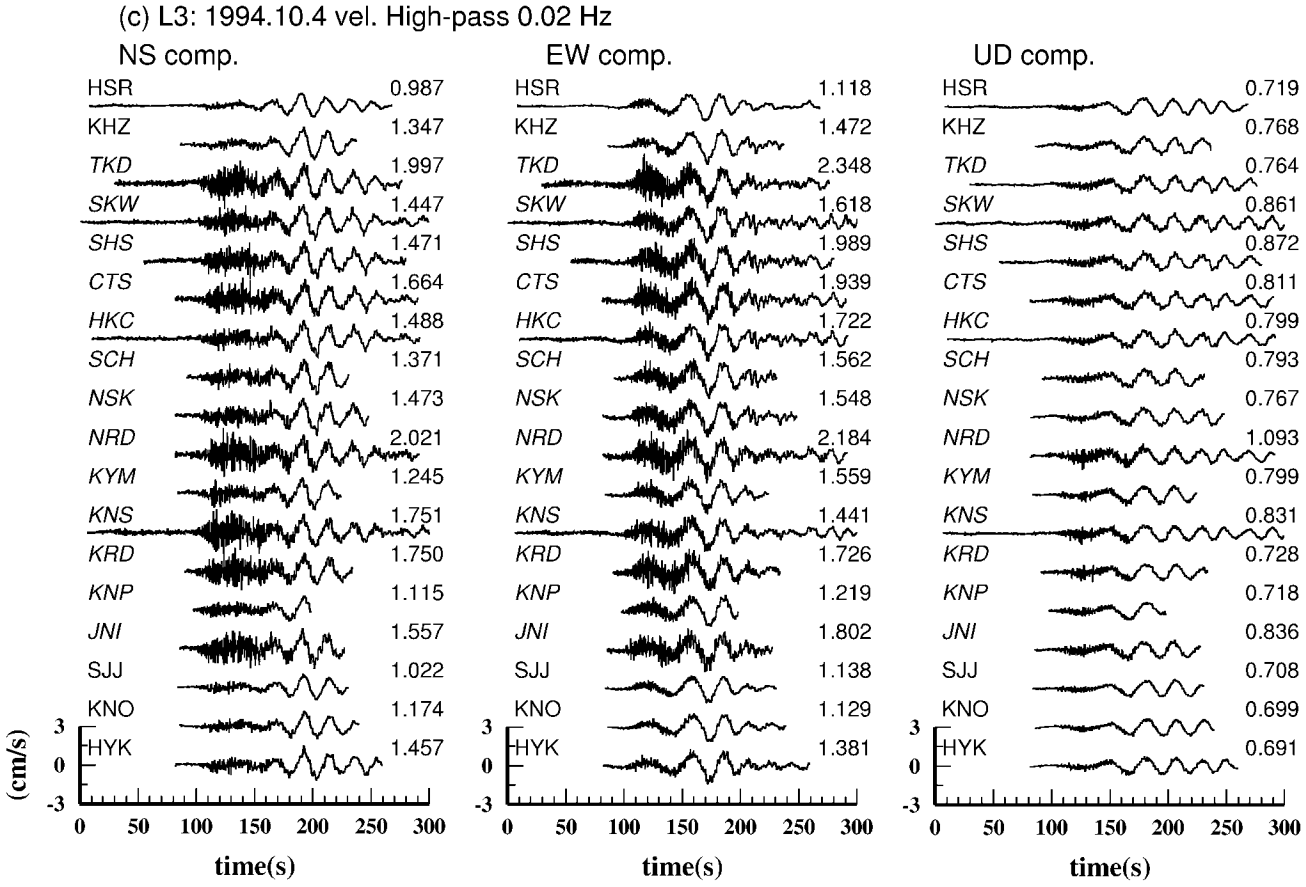

Figure 4. Continued.

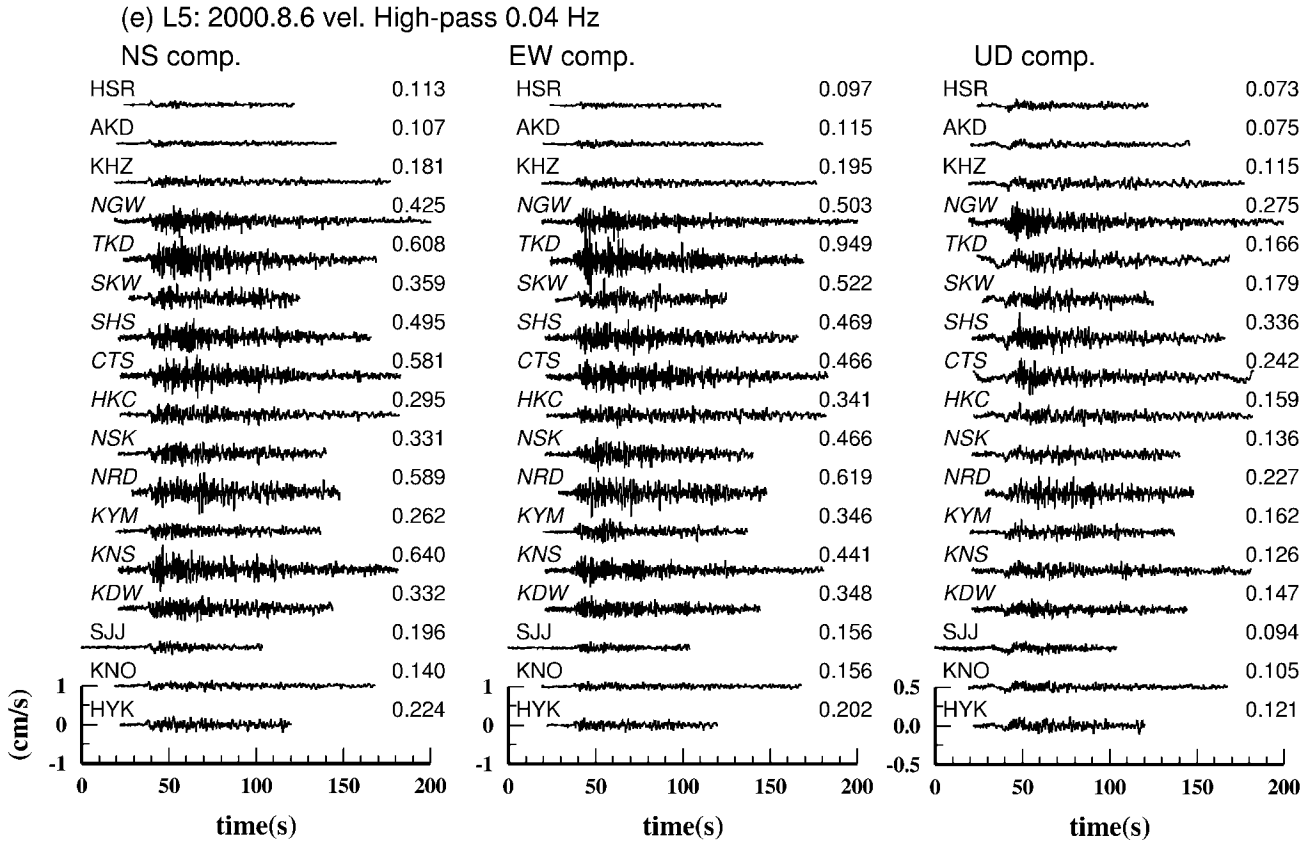

Figure 4. Continued.

Chavez-Garcia (1993). The geometrical averages of HVRs are compared with those of HHRs in Figure 10. The large deviations of HVRs in the low-frequency range may be attributed, in part, to *SV*-wave incidences with different angles, even if the simple interpretation of HVRs (Nakamura, 1988) is valid. HVRs at sediment sites are similar to HHRs at frequencies higher than 0.5 Hz. However, the HVR at NRD underestimates by a factor of 2, and those at CTS, SHS, and TKD are also smaller than HHRs, even at higher frequencies. On the contrary, HVRs at rock sites strongly overestimate HHRs without exception. The HVRs for KNO have a peak at about 0.2 Hz and there are no significant troughs at about 0.2 Hz in HVRs at the sediment sites despite the significant peak in spectral ratios of the up–down component as shown in Figure 7c. These results suggest that the frequency response of up–down component at KNO have a trough as shown in Figure 6 (panel 3) and the trough makes the peaks at about 0.2 Hz as shown in Figure 7c.

Satoh *et al.* (2001) examined the differences of empirical site amplification using different time windows, such as *S* waves, *P* waves, coda, and microtremors. They showed that HVRs for the *S*-wave portions are different from HHRs, whereas HVRs are consistent with theoretical HVRs for obliquely incident (30°) *SV* waves. They also indicated that the *S*-coda portions at soft-sediment sites are mixed with surface waves and that the *S*-coda HVRs in frequencies lower than 3 Hz may be interpreted by the fundamental mode of Rayleigh waves.

Because of the long time window used in our analysis, HHRs in the present results reflect not the amplification factor of *S* waves alone, but the empirical-site factors, including secondary generated surface waves. Judging from the stability and similarity of HVRs with HHRs, HVRs may be used as substitutes for HHRs in frequencies higher than 0.5 Hz for the empirical-site amplification factors. However, at the same time, the deviations of HVR at sediment sites are very large at frequencies lower than 0.5 Hz and, at rock sites, overestimate the site amplification factor. The large deviations of HVRs at low frequencies may be attributed to the variations of incident angles of seismic motion; therefore, the average of HVRs at low frequency may not be meaningful. However, the average has a certain meaning if plural incident angles have to be considered because of multipath incoming waves from distant events.

Site Factors Evaluated by the Generalized Inversion Method

In this section, we compared the site factors obtained by the first method (HHRs) with those estimated by the generalized inversion method (Iwata and Irikura, 1988) using small local events. We analyzed moderate ground motions

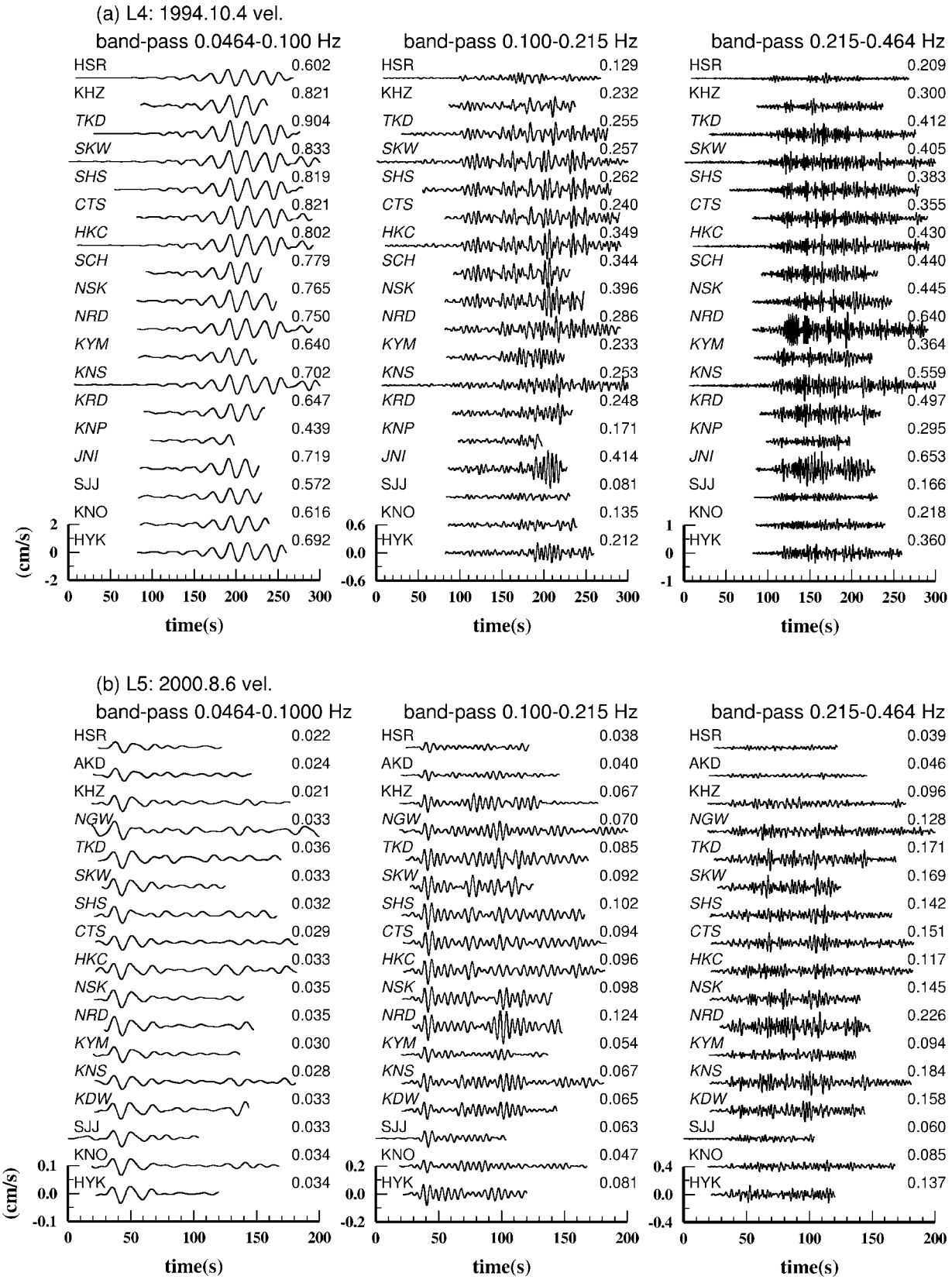

Figure 5. North–south components of bandpass-filtered velocity seismograms. The top plots are waveforms for L3, and the bottom plots are for L5. The letters written on the left side of the waveforms indicate station code, and the numbers written on the right side of waveforms are the PGV values of the waveforms.

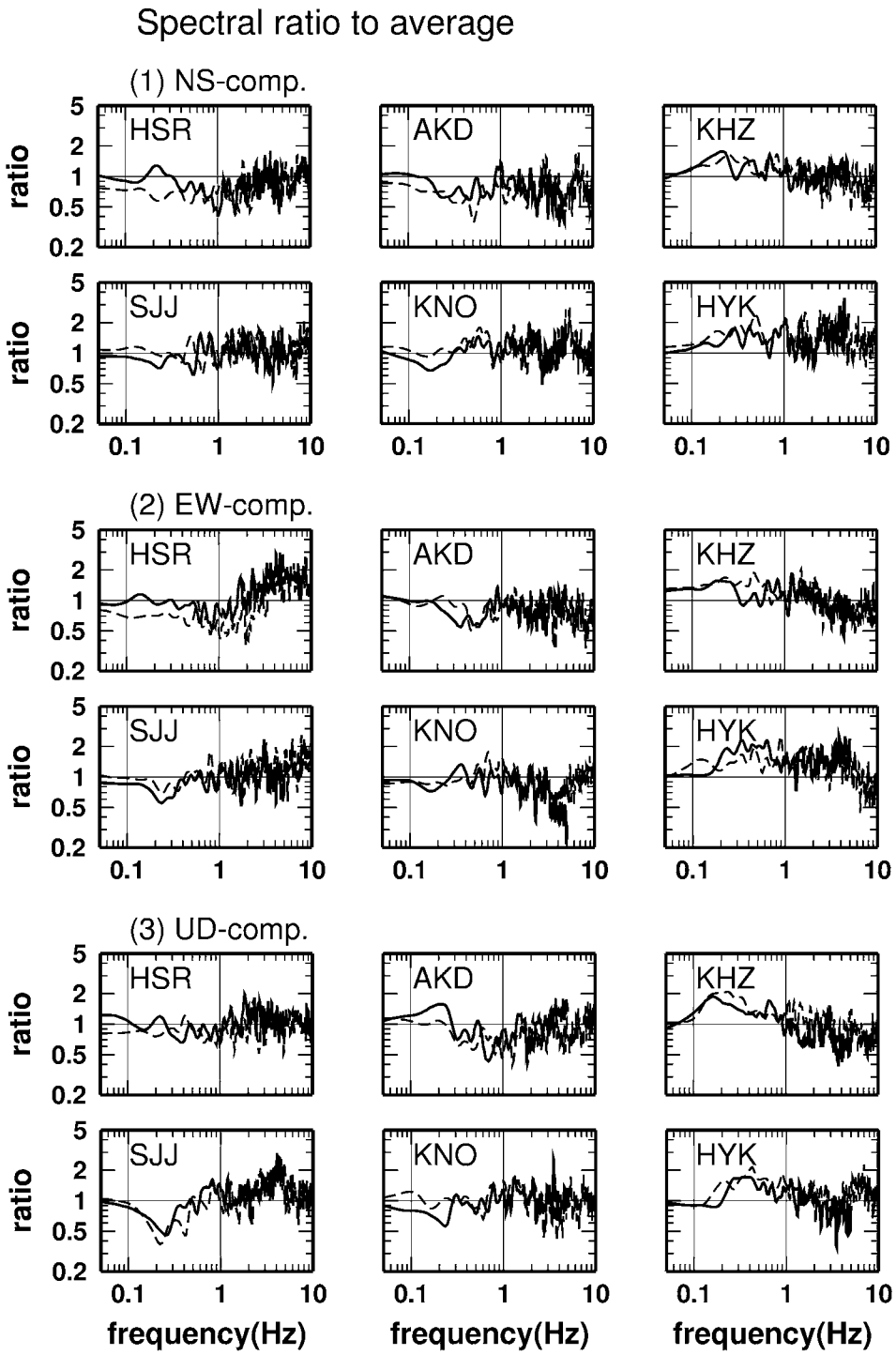

Figure 6. Fourier spectral ratios of each rock site with respect to the average of all sites. Panels 1, 2, and 3 show the results for the north–south (NS), east–west (EW), and up–down (UD) components, respectively. Thick lines and broken lines represent the ratio to the average spectra of events L4 and L5 in Table 1, respectively.

at 31 sites, from 9 events that occurred near Ashigara valley, as shown in Table 4. These earthquakes are mostly shallow, with magnitudes from 4.0 to 5.5, as shown in Table 3. The location of observation sites and epicenters are shown in Figure 2.

The observed *S*-wave Fourier amplitude spectrum is expressed by,

$$O_{ij}(f) = S_i(f) \cdot R_{ij}^{-1} \cdot \exp(-\pi R_{ij} f / Q_s(f) v_s) \cdot G_j(f), \quad (3)$$

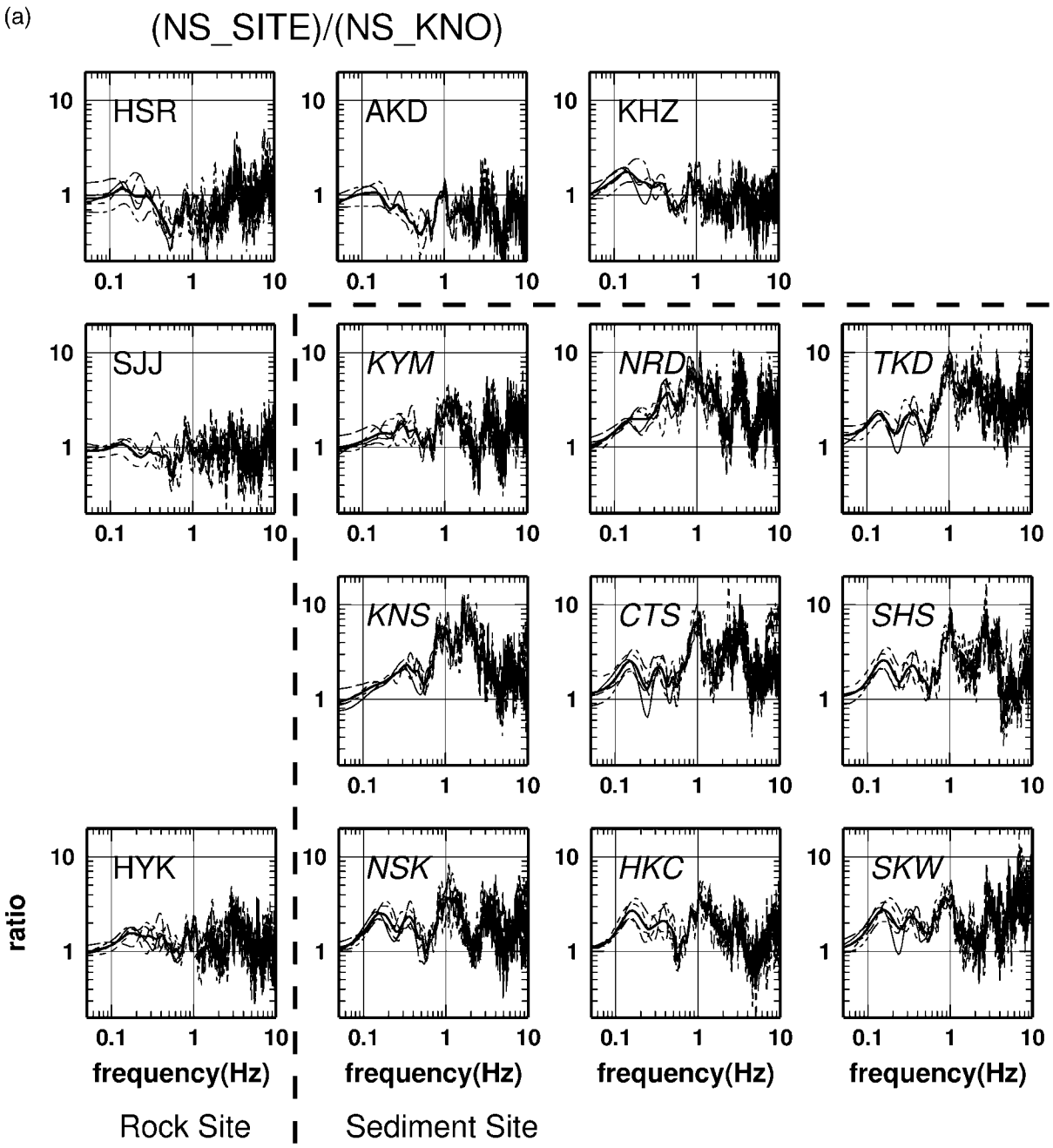

Figure 7. Fourier spectral ratios or amplification factors of the strong-motion sites with respect to KNO. (a), (b), and (c) show the result for the north–south (NS), east–west (EW), and up–down components, respectively. Only stations with more than three events retrieved are displayed. The spectral ratio for each event and their average are displayed. These spectral ratios were smoothed by Parzen windows of 0.1-Hz widths. (*continued*)

where $O_{ij}(f)$ is the observed *S*-wave Fourier amplitude spectrum of the *i*th event at the *j*th station; $S_i(f)$ is the source amplitude spectrum of the *i*th event; $G_j(f)$ is the site amplification factor at the *j*th station; R_{ij} is the source distance between the *i*th event and the *j*th station; $Q_s(f)$ is the average Q_s-value along the wave propagation path; and v_s is the average *S*-wave velocity along the wave propagation path ($=$ 3.5 km/sec). Equation (3) is modified into a linear form by taking its logarithm. Source spectra, Q_s-value, and site amplification factor at each station are obtained in a least-squares sense by the linear inversion method. As a constraint condition, we assigned the KNO rock site as the reference site and set the site amplification factor for KNO to be 2, irrespective of frequency. We analyzed the *S*-wave portions of two horizontal components (north–south and east–west) using the time windows (cosine tapered) of 5 sec and 10 sec

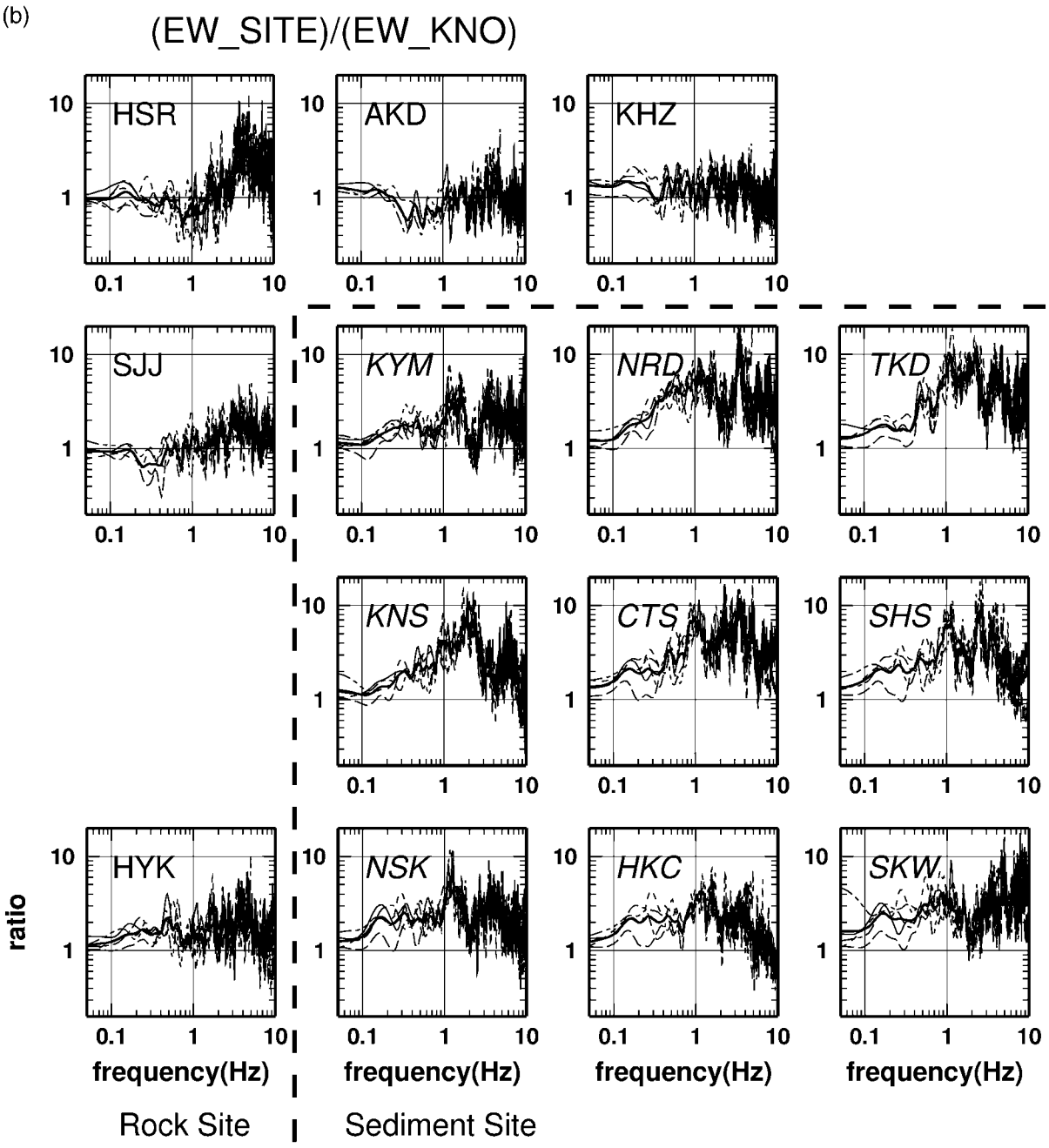

Figure 7. Continued.

after the onset of the *S* waves. Velocity spectra obtained by vectorial summation of the two horizontal components are then used. We restrict our discussion in the over-0.5-Hz frequency range because of the low S/N for frequencies lower than 0.5 Hz.

Results of the analysis are summarized as follows. The Q_s-value of basement rock in the 0.5- to 1-Hz frequency range is about 20, whereas $Q_s(f) = 20f$ fits the data in the frequency range from 1 to 15 Hz. This value is very small relative to the results from shallow earthquakes occurring in the Kanto or Tohoku district, Japan (e.g., Kato *et al.*, 1992). However, in this article, our concern is to determine the site factor and not the Q_s itself. Because the bedrock Q_s-value does not affect relative site factors, we will not go into detail on this in this article.

The site amplification factors evaluated by the inversion method are shown in Figure 11 for the two time-window durations, together with two components average of HHRs of large events (Fig. 7) obtained by geometrical averaging of the horizontal components from large, distant events. Site factors by the two different methods are similar for both rock and sediment sites; however, peak levels of inversion results at about 1 Hz are smaller than HHRs at several sediment sites (TKD, KNS, CTS, and SHS). These peak levels of

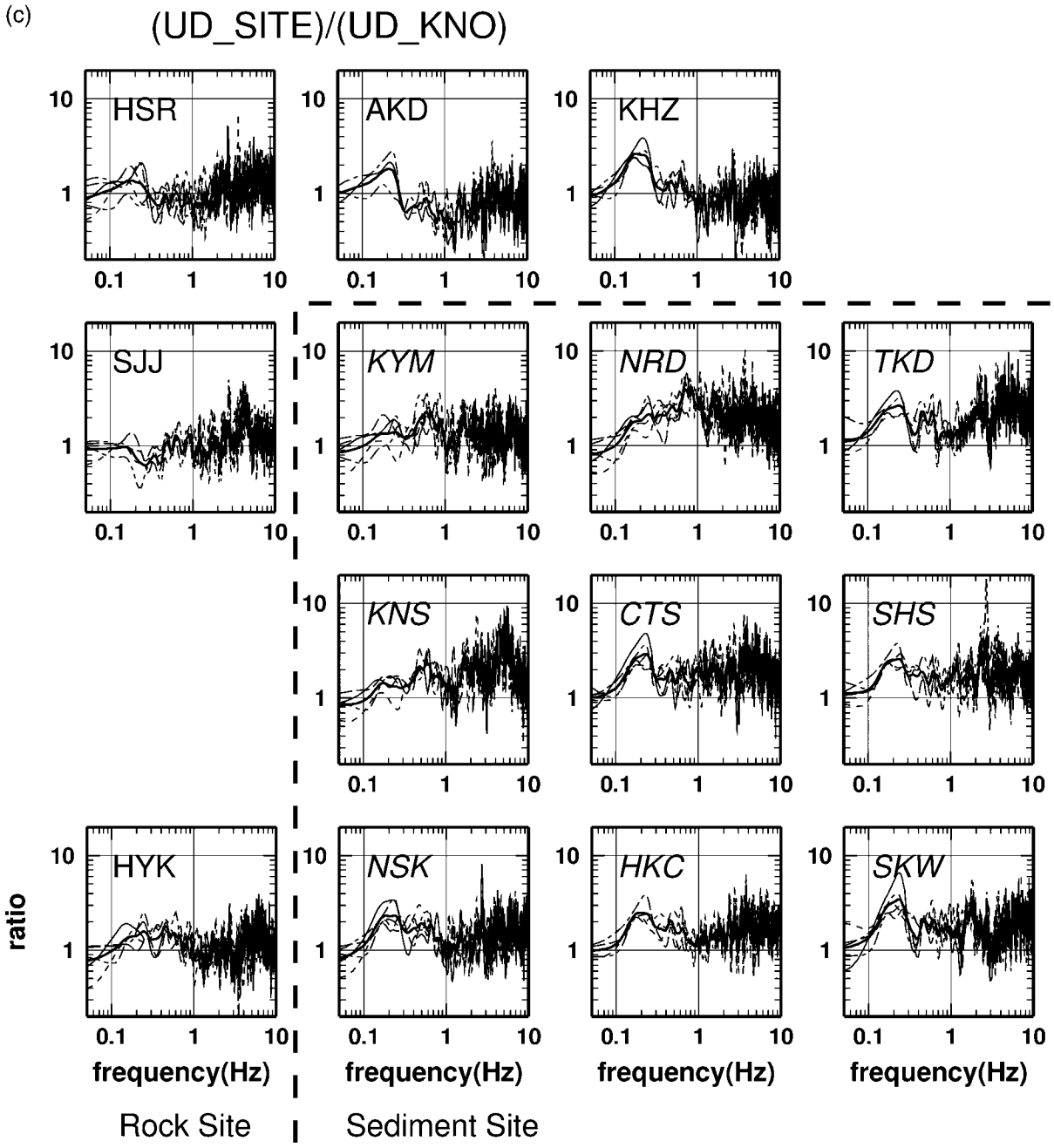

Figure 7. Continued.

inversion results, however, tend to increase slightly with the length of the time window. Thus, in the time window of 10 sec, they approach the HHRs as shown by the broken lines in Figure 11. These results are similar to those of previous studies at different sites (e.g., Field and Jacob, 1995; Satoh *et al.*, 2001). This may be because of the effects of later arrivals of surface waves in the case of a long time window. The spectral ratio method using large, distant events (HHRs) is advantageous in empirically assessing site effects, including the effects of secondary generated waves in a basin, owing to the use of long time windows. In frequencies higher than 2 Hz, however, no significant change of amplification factors are found, irrespective of the length of time windows except for TKD. This implies that 1D analysis or estimation is applicable for high-frequency motions over 2 Hz. On the contrary, site factors at about 1 Hz motion in sediment sites have to be carefully assessed considering 2D/3D effects.

Discussion

As mentioned in the preceding section, 1D analysis may be able to explain the empirical-site factor in frequencies

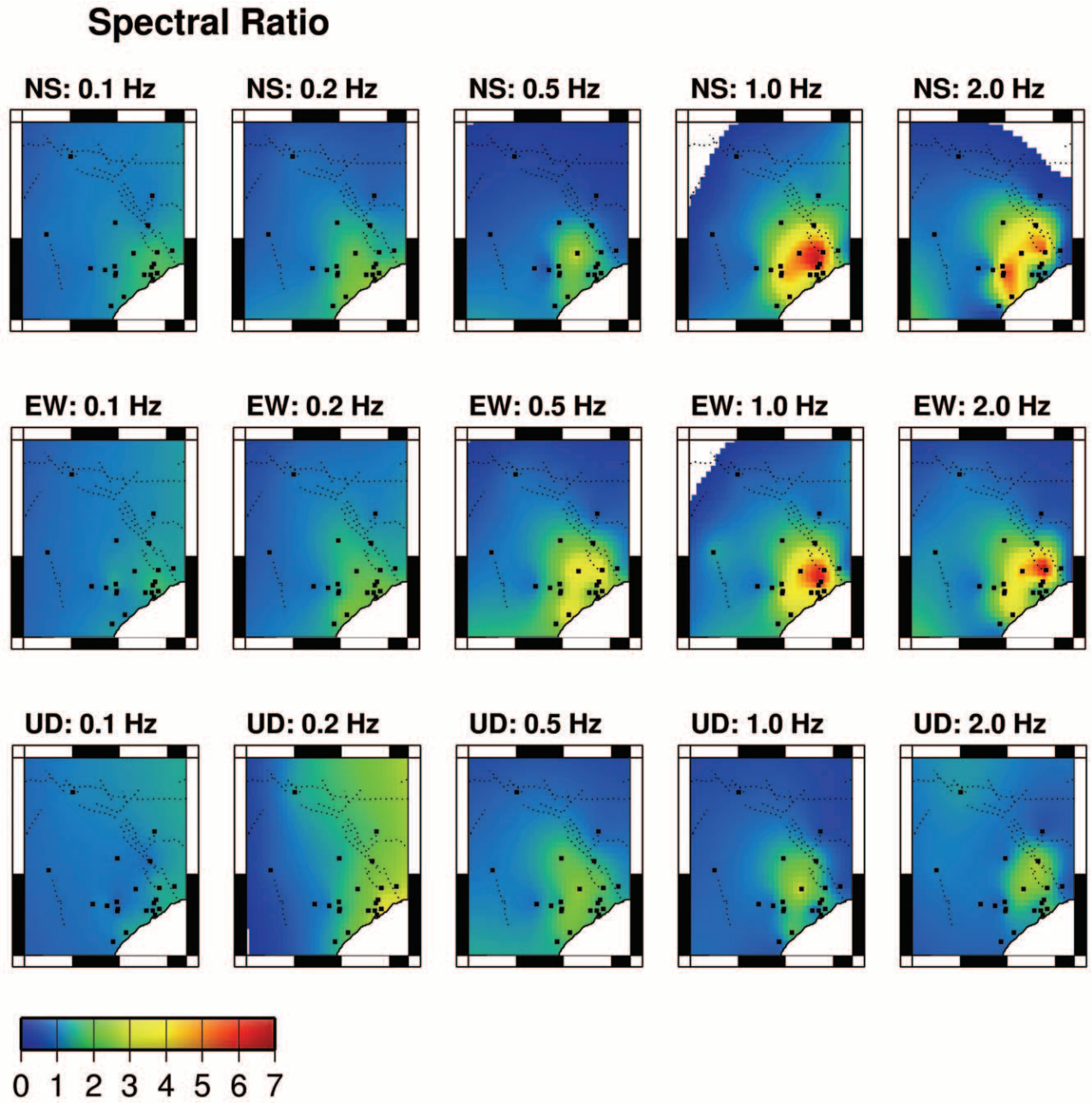

Figure 8. Spatial variations of spectral ratios with respect to KNO or site amplification factors. Filled squares indicate the observation stations. GMT (Wessel and Smith, 1998) was used for spatial interpolation and for drawing these figures.

higher than 2 Hz. We conducted 1D analysis for four sediment sites using the underground structure models based on *PS*-logging data shown in Table 5. The model for CTS is based on *PS* logging (e.g., Kudo and Shima, 1988) to a depth of 467 m but is modified by Saito *et al.* (1995) with the method for optimizing the spectral ratio of vertical array observation data. At the same time, the Q_s-model for CTS was also obtained. The KNO located on outcrop of rock has a V_s = 1200 m/sec (e.g., Sawada, 1992), which is almost equal to the bottom of the borehole at CTS. For other sites, the data within the bold lines in Table 5 are determined by *PS* logging, whereas other parameters are assumed using the CTS model. The different estimates of HHR for the sites in Table 5 are compared in Figure 12. Those obtained from large-event data are shown by thick solid lines, site factors estimated by generalized inversion using a time window of 5 sec are shown by thin lines, and amplitude factors calculated from the basement layer with V_s = 1260 m/sec are shown by dotted lines. Because *S* waves propagate almost vertically toward the low-velocity surface layers, we assumed vertically incident *SH* waves in the calculation. Although 1D *SH* responses cannot represent some peaks, the

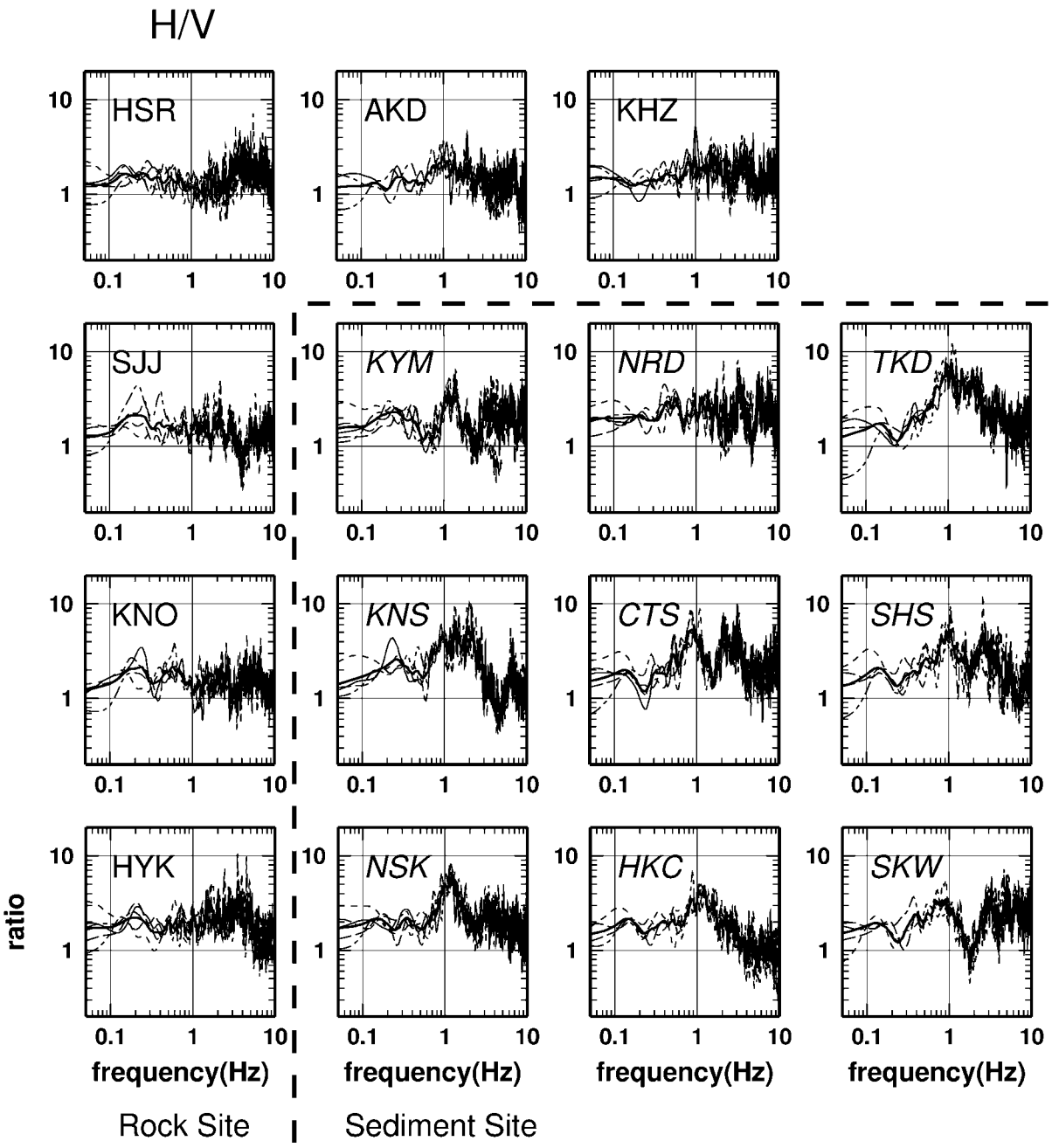

Figure 9. Fourier spectral ratios of horizontal to vertical components at each station. Only the stations with more than three events retrieved are displayed. The spectral ratio for each event and their average are displayed.

spectral shapes of site factors roughly match with HHRs by the generalized inversion in frequencies higher than 2 Hz. We will not go into detail, but tuning of the model parameters, especially for the Q_s-values, may give better agreement.

In general, empirical-site factors are affected by the reference-site responses. Kato *et al.* (1992) showed that the difference between the constraint condition and the reference-site response gave a systematic discrepancy between the site factors and 1D analysis results using vertical array data. In fact, some discrepancies of HHR exist between 1D *SH* responses and inversion results, as shown in Figure 12. The peaks at about 1 Hz by the inversion results are systematically larger than those of the 1D analysis, whereas discrepancies in the high-frequency range are not so large and systematic. The discrepancy at about 1 Hz may be produced by the site effects of KNO and some factors that cannot be modeled by 1D analysis. HHRs estimated by large and remote events tend to overestimate those from 1D responses and inversion. This will be attributed to the effects

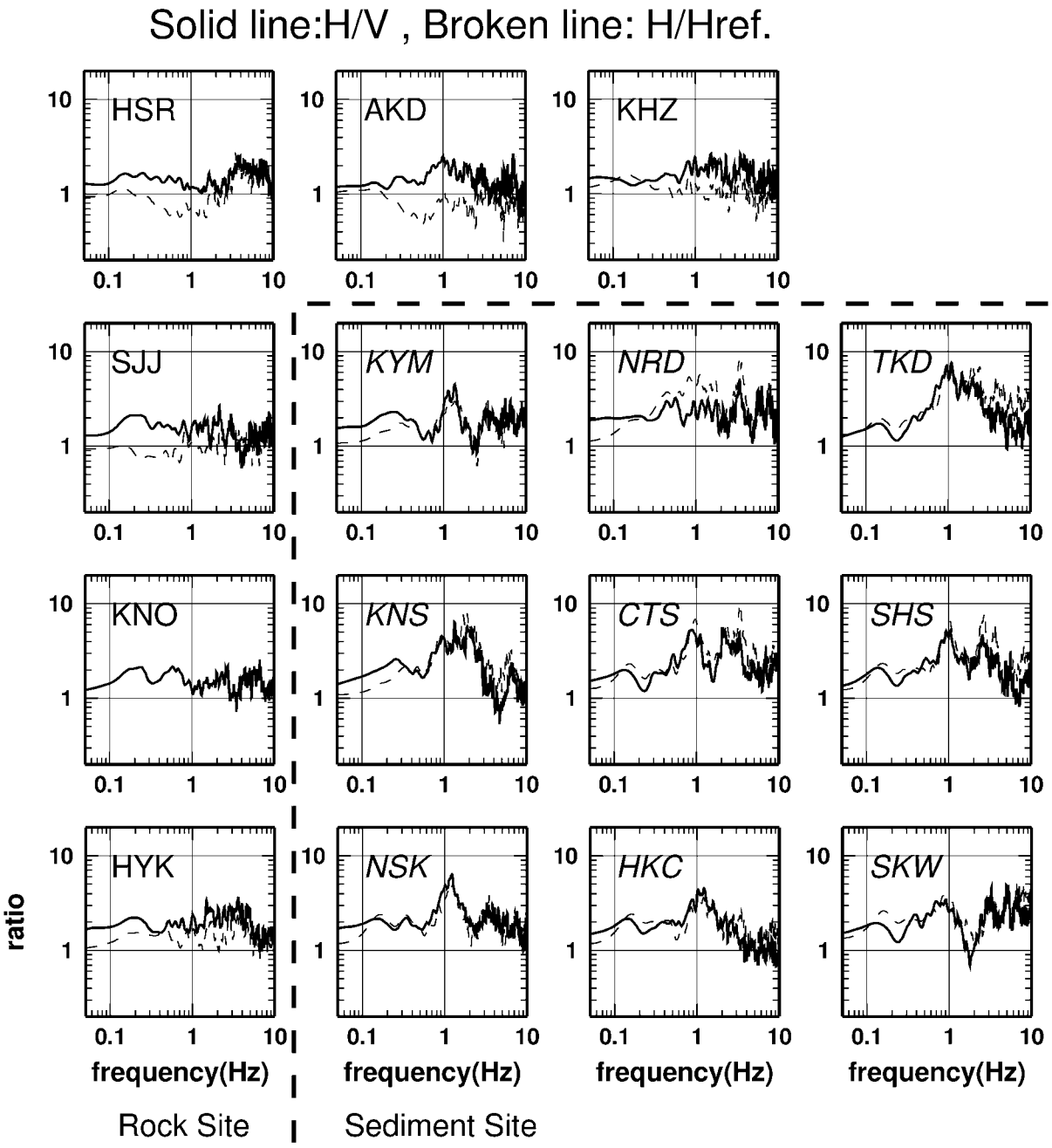

Figure 10. Comparison of HVR and HHR. Solid and broken lines denote HVR and HHR, respectively.

of secondary generated waves in the basin. We have to consider these factors; however, we may say that it is adequate to select KNO as a reference site for evaluating site responses. This is because the response of KNO shows nearly average response among the rock sites, as shown in Figure 6, and the deviation among the rock site responses is smaller than the deviation between rock and sediment sites, as shown in Figure 7. In detail the rock sites surrounding Ashigara Valley show the different site responses; therefore, it is important for precise assessments or detailed discussions to select a proper reference site.

Conclusions

The site effects in and around Ashigara Valley were evaluated using records from large, distant events. Site amplification factors for both rock and sediment sites were evaluated by taking spectral ratios with respect to one rock site (KNO). A long time window of 81.92 sec was used for obtaining the spectra of earthquake motions, so that the spectral ratios relative to KNO give empirical amplification factors that include the effects of secondary generated waves in the basin. These amplification factors do not discriminate be-

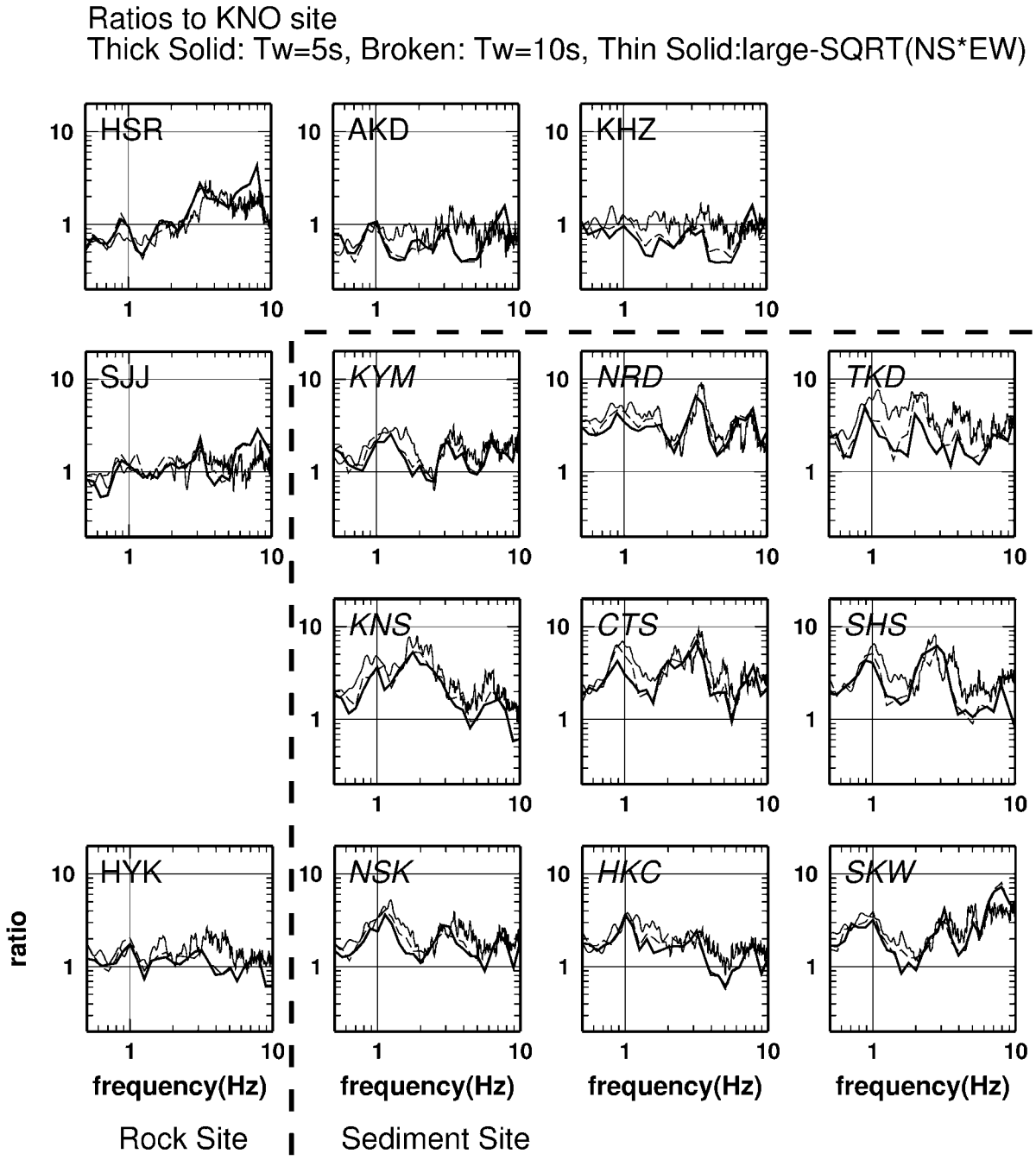

Figure 11. Site amplification factors with respect to the rock site KNO. Thick solid and broken lines show the results of inversion analysis for the time windows of 5 sec and 10 sec, respectively. Thin solid lines show the geometrical average of spectral ratios for the two horizontal components obtained from remote large events (Fig. 7).

tween wave types or amplification mechanism, although they should be regarded as essential in earthquake hazard assessment, at least in cases where earthquake motions of almost vertical incidence can be modeled. In the analysis, two shallow events were included; therefore, the incidence of surface waves to the valley should also be taken into account. In fact, surface waves were clearly found in the data (L3), but they are predominantly in the low-frequency range between 0.03 and 0.04 Hz, and such low-frequency waves are not affected by the heterogeneity of surface and underground structures near Ashigara Valley. On the other hand, the higher-frequency motions from the shallow events dominated in the early arrivals of *S* waves; thus, the assumption of quasivertical incidence of waves is allowable. We mapped the obtained site amplification factors as a function of frequency. The spectral ratios tend to be large toward the south-

Table 5
Underground Velocity Structure Models for Several Sediment Sites

Thickness (m)	V_p (m/sec)	V_s (m/sec)	Density (g/cm^3)	$Q_s = Q_0 * f ** n$	
				Q_0	n
CTS					
10	800	110	1.2	2.0	0.8
15	1650	220	1.7	3.0	0.7
25	1650	250	1.7	4.0	0.6
15	1650	330	1.9	6.0	0.6
25	1960	560	2.0	7.0	0.6
150	2250	790	2.1	10.0	0.8
180	2350	970	2.2	10.0	0.8
—	2520	1260	2.3	10.0	0.8
NRD					
8	1300	120	1.2	2.0	0.8
10	1300	180	1.2	2.0	0.8
4	1660	300	1.9	6.0	0.6
20	1530	210	1.7	4.0	0.6
15	1850	630	2.0	10.0	0.6
150	2250	790	2.1	10.0	0.8
180	2350	970	2.2	10.0	0.8
—	2520	1260	2.3	10.0	0.8
TKD					
2	350	110	1.2	2.0	0.8
12	900	110	1.2	2.0	0.8
6	1550	240	1.7	3.0	0.7
6	1550	330	1.9	6.0	0.6
5	1550	250	1.7	6.0	0.6
45	1640	350	1.9	6.0	0.6
25	1960	560	2.0	7.0	0.6
150	2250	790	2.1	10.0	0.8
180	2350	970	2.2	10.0	0.8
—	2520	1260	2.3	10.0	0.8
KNS					
7	600	65	1.5	2.0	0.8
5	1500	170	1.5	3.0	0.7
16	2100	690	2.0	4.0	0.6
48	1650	400	1.9	6.0	0.6
6	2300	750	2.0	6.0	0.6
12	1800	400	1.9	7.0	0.6
80	2300	700	2.2	10.0	0.8
180	2350	970	2.2	10.0	0.8
—	2520	1260	2.3	10.0	0.8

The model for CTS was determined by Saito *et al.* (1995). The other three site models are basically the same as the CTS model, except that original *PS*-logging data were used for the shallow part (shaded areas).

east area of the valley for the low-frequency range below 0.5 Hz. The area showing large amplification factors at about 1 Hz and at higher frequencies is localized near the southeast of the valley.

HVRs, using the same time windows as the reference-site method, were compared with the spectral ratios of horizontal motions (HHRs). HVRs at rock sites are not always equal to unity and vary between 1 and 3 against frequency. Moreover, the deviation from event to event is large, and the averages of HVRs, in general, are larger than HHRs. HVRs in the frequency range higher than 0.5 Hz coincide with HHRs at many sediment sites, but no systematic relationship could be seen at lower frequencies. By restricting the scope to the frequency range higher than 0.5 Hz, HVRs may be used as substitutes for HHRs in determining the empirical-site amplification factors of sediment sites. However, this method should be used with caution, because the applicability of HVRs may be valid only for soft sediments and the reliable frequency range depends on the site conditions.

Site effects were also evaluated by the generalized inversion method using data from local small events, restricted in the frequency range higher than 0.5 Hz. Site factors estimated by the inversion method coincide with HHRs from large events in the frequency range higher than 2 Hz. However, the spectral peaks at about 1 Hz of sediment sites by the inversion method are lower than those of HHRs.

The horizontal spectral ratio to a reference site (HHR), horizontal-to-vertical (HVR), and generalized inversion methods give similar results if restricted in the higher frequency of over 2 Hz, with the amplification factors explained by 1D responses. For the low-frequency range, basin-induced or transduced surface waves may affect site responses as basin effects.

Acknowledgments

We sincerely thank Mr. Takahashi and Mr. Sakaue of ERI for their efforts to maintain the Ashigara Valley observation system and to retrieve the strong-motion data. We are grateful to NIED, CRIEPI, and TEPCO for providing the observation data. We also thank Dr. T. Satoh, the anonymous reviewer, and associate editor Dr. H. Kawase for their valuable comments in improving this article. Many figures were prepared with Generic Mapping Tools developed by Wessel and Smith (1998).

References

Andrews, D. J. (1982). Separation of source and propagation spectra of seven Mammoth Lake aftershocks, in *Proceedings of Workshop 16, Dynamic Characteristics of Faulting, 1981*, *U.S. Geol. Surv. Open-File Rept. 82-591*, 437.

Boatwright, J., J. B. Fletcher, and T. E. Fumal (1991). A general inversion scheme for source, site, and propagation characteristics using multiply recorded sets of moderate-sized earthquakes, *Bull. Seism. Soc. Am.* **81,** 1754–1782.

Bonilla, L. F., J. H. Steidl, G. T. Lindley, A. G. Tumarkin, and R. J. Archuleta (1997). Site amplification in the San Fernando Valley, California: variability of site-effect estimation using the S-wave, coda, and H/V methods, *Bull. Seism. Soc. Am.* **87,** 710–730.

Borcherdt, R. D. (1970). Effects of local geology on ground notion near San Francisco Bay, *Bull. Seism. Soc. Am.* **60,** 29–81.

Field, E. H., and K. H. Jacob (1995). A comparison test of various site-response estimation techniques, including three that are not reference-site dependent, *Bull. Seism. Soc. Am.* **85,** 1127–1143.

Imamura, A. (1929). On the earth-vibrations induced in some localities at the arrival of seismic waves, *Bull. Earthquake Res. Inst. Tokyo Univ.* **7,** 489–494.

Ishimoto, M. (1932). Comparaison accelerometrique des secousses sismiques dans deux parties de la ville de Tokyo, *Bull. Earthquake Res. Inst. Tokyo Univ.* **10,** 171–187.

Iwata, T., and K. Irikura (1988). Source parameters of the 1983 Japan Sea earthquake sequence, *J. Phys. Earth* **36,** 155–184.

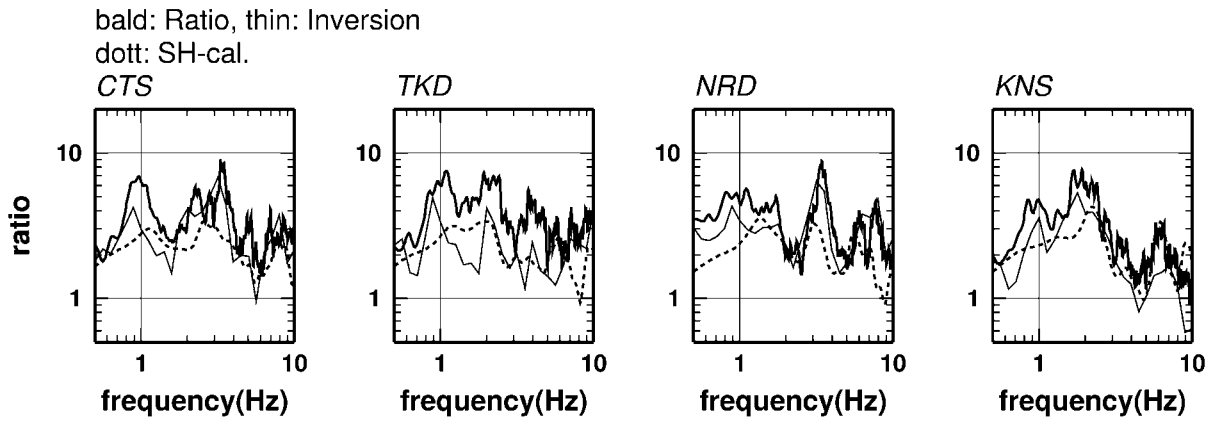

Figure 12. Comparison between spectral ratios from the horizontal components with reference to KNO, the generalized inversion results, and the calculated transfer functions from the layer with V_s = 1260 m/sec. Bold lines show the geometrical average of two horizontal spectral ratios. Thin lines show the site factors estimated by generalized inversion. Dotted lines show the response from vertical incident *SH* waves for the underground structure models in Table 5.

Kato, K., M. Takemura, T. Ikeura, K. Urao, and T. Uetake (1992). Preliminary analysis for evaluation of local site effects from strong motion spectra by an inversion method, *J. Phys. Earth* **40,** 175–191

Kawase, H., and T. Sato (1992). Simulation analysis of strong motions in the Ashigara valley considering one-and two-dimensional geological structures, *J. Phys. Earth* **40,** 27–56.

Kinoshita, S. (1998). Kyoshin Net (K-NET), *Seism. Res. Lett.* **69,** 309–332.

Kudo, K. (1992). Earthquake motions: given and blinded data, *Proc. Intern. Symp. on the Effects of Surface Geology on Seismic Motion, Odawara, Japan* **2,** 53–60.

Kudo, K., and E. Shima (1988). Installation of strong motion seismographs, plan for geotechnical measurements, at Ashigara valley site effects test area, Japan, in *Proceedings of the IASPEI/IAEE Joint Working Group on Effects of Surface Geology on Seismic Motion, Second Workshop, Tokyo, Japan*, Japanese Working Group on Effects of Surface Geology on Seismic Motion, II-1–II-11.

Kudo, K., E. Shima, and M. Sakaue (1988). Digital strong motion accelerograph array in Ashigara valley, *Proc. 9th World Conf. Earthquake Eng., Tokyo, Japan* **8,** 119–124.

Kudo, K., and Y. Sawada (1998). A brief review on the Ashigara Valley blind prediction test and some follow-up studies, in *The Effects of Surface Geology on Seismic Motion*, K. Irikura, K. Kudo, H. Okada, and T. Sasatani (Editors), Balkema, Rotterdam, The Netherlands, 305–312.

Lermo, J., and F. J. Chavez-Garcia (1993). Site effects evaluation using spectral ratios with only one station, *Bull. Seism. Soc. Am.* **83,** 1574–1594.

Nakamura, Y. (1988). Inference of seismic responses of surface layer based on Microtremor measurement, *Quarterly Report on Railway Research* **4,** 18–27 (in Japanese).

Riepl, J., P.-Y. Bard, D. Hatzheld, C. Papaionnou, and S. Nechtschein (1998). Detail evaluation of site response estimation methods across and along the sedimentary valley of Volvi (EURO-SEISTEST), *Bull. Seism. Soc. Am.* **88,** 488–502.

Saito, S., T. Sasatani, and K. Kudo (1995). Attenuation characteristics of S waves in the sedimentary layers at the Ashigara Valley, *Geophys. Bull. Hokkaido Univ., Sapporo, Japan*, **58,** 39–61 (in Japanese).

Sasatani, T., M. Ikeda, and N. Sakajiri (1992). A study of site effects by means of strong motion seismograms from near by, intermediate depth earthquake, *J. Phys. Earth* **40,** 85–98.

Sato, K., S. Higashi, H. Yajima, and S. Sasaki (1998). Ashigara valley test site, 1D or 2D-3D? in *The Effects of Surface Geology on Seismic Motion*, K. Irikura, K. Kudo, H. Okada, and T. Sasatani (Editors), Balkema, Rotterdam, The Netherlands, 319–340.

Satoh, T., H. Kawase, and S. Matsushima (2001). Differences between site characteristics obtained from microtremors, S-waves, P-waves, and Codas, *Bull. Seism. Soc. Am.* **91,** 313–334.

Sawada, Y. (1992). Geotechnical data, *Proc. Intern. Symp. on the Effects of Surface Geology on Seismic Motion, Odawara, Japan* **2,** 29–42.

Seekins, L. C., L. Wennerberg, L. Margheriti, and H.-P. Liu (1996). Site amplification at five locations in San Francisco, California: a comparison of S waves, codas, and microtremors, *Bull. Seism. Soc. Am.* **86,** 627–635.

Smith, W. H. F., and P. Wessel (1990). Gridding with continuous curvature splines in tension, *Geophysics* **55,** 293–305.

Steidl, J. H., A. G. Tumarkin, and R. J. Archulata (1996). What is a reference site?, *Bull. Seism. Soc. Am.* **86,** 1733–1748.

Uetake, T., and K. Kudo (1998). Evaluation of site effects in a wide frequency band at Ashigara Valley, Japan, using strong motion records from remote and large events, *Zisin, 2nd Ser.* **50,** 397–414 (in Japanese).

Wessel, P., and W. H. F. Smith (1998). New, improved version of the Genetic Mapping Tools released, *EOS Trans. AGU* **79,** 579.

Yamazaki, H. (1992). Tectonics of a plate collision along the northern margin of Izu peninsula, central Japan, *Bull. Geol. Surv. Jpn.* **43,** 603–657.

Yamazaki, F., and M. A. Ansary (1997). Horizontal-to-vertical spectrum ratio of earthquake ground motion for site characterization, *Earthquake Eng. Struct. Dyn.* **26,** 671–689.

Seismic Design Group, R&D Center
The Tokyo Electric Power Company, Inc.
4-1, Egasaki-cho, Tsurumi-ku
Yokohama 230-8510, Japan
(T.U.)

Earthquake Research Institute
The University of Tokyo
1-1-1, Yayoi, Bunkyo-ku
Tokyo 113-0032, Japan
(K.K.)

Manuscript received 8 April 2004.